RESEARCH ARTICLE

NANO · MICRO small
www.small-journal.com

Hybrid Nanogel-Wrapped Anisotropic Gold Nanoparticles Feature Enhanced Photothermal Stability

David Esporrín-Ubieto, Cristián Huck-Iriart, Agustin S. Picco, Ana Beloqui, and Marcelo Calderón**

Anisotropic gold nanoparticles (AuNPs) are renowned for their unique properties – including localized surface plasmon resonance (LSPR) and adjustable optical responses to light exposure – that enable the conversion of light into heat and make them a promising tool in cancer therapy. Nonetheless, their tendency to aggregate and consequently lose their photothermal conversion capacity during prolonged irradiation periods represents a central challenge in developing anisotropic AuNPs for clinical use. To overcome this issue, an innovative approach that facilitates the encapsulation of individual anisotropic AuNPs within thin nanogels, forming hybrid nanomaterials that mirror the inorganic core's morphology while introducing a negligible (2–8 nm) increase in overall diameter is proposed. The encapsulation of rod- and star-shaped anisotropic AuNPs within poly-acrylamide (pAA) or poly-(N-isopropylacrylamide) (pNIPAM) nanogels is successfully demonstrated. The ultrathin polymeric layers display remarkable durability, significantly enhancing the photothermal stability of anisotropic AuNPs during their interaction with near-infrared light and effectively boosting their photothermal capacities for extended irradiation periods. The outcomes of the research thus support the development of more stable and reliable AuNPs as hybrid nanomaterials, positioning them as promising nanomedicinal platforms.

1. Introduction

Tunable gold nanoparticles (AuNPs) have wide-ranging applications in diagnostics, drug delivery, therapy, and imaging.[1] Anisotropic AuNPs have garnered significant interest due to their distinct optical properties, including their capacity to convert light into heat.[2] Adjusting the size and shape of AuNPs can modulate their optical properties, which are marked by localized surface plasmon resonance (LSPR); spherical AuNPs exhibit maximum absorption in the visible range of the spectra, while anisotropic AuNPs display excitation in the near-infrared region.[3,4] This spectral window – spanning 700–1100 nm – holds significance for photothermal therapy as this range aligns with biologically transparent wavelengths.[5] Hence, successful therapeutic approaches that leverage the ability of anisotropic AuNPs to convert light into confined thermal energy have been evaluated in animal models.[6–8] Rastinehad et al., demonstrated the eradication of prostate tumors in 14/16 patients through localized injections of gold-coated spherical silicon nanoparticles followed by irradiation with near-infrared light.[9] While this achievement underscores the notable photothermal features of AuNPs in disease treatment, the perhaps more significant potential of anisotropic AuNPs remains unexplored regarding clinical translation.

The lack of anisotropic AuNP stability under prolonged light exposure limits their implementation in localized photothermal

D. Esporrín-Ubieto, A. Beloqui, M. Calderón
POLYMAT
Applied Chemistry Department, Faculty of Chemistry
University of the Basque Country UPV/EHU
Paseo Manuel de Lardizabal 3, Donostia-San Sebastián 20018, Spain
E-mail: ana.beloquie@ehu.eus; marcelo.calderonc@ehu.eus

C. Huck-Iriart
ALBA Synchrotron Light Source
Carrer de la Llum 2–26, Cerdanyola del Vallès 08290, Barcelona, Spain

A. S. Picco
Instituto de Investigaciones Fisicoquímicas, Teóricas y Aplicadas (INIFTA)
Universidad Nacional de La Plata (UNLP) – CONICET
Diagonal 113 y Calle 64, La Plata 1900, Argentina

A. Beloqui, M. Calderón
IKERBASQUE
Basque Foundation for Science
Plaza Euskadi 5, Bilbao 48009, Spain

The ORCID identification number(s) for the author(s) of this article can be found under https://doi.org/10.1002/smll.202404097

DOI: 10.1002/smll.202404097

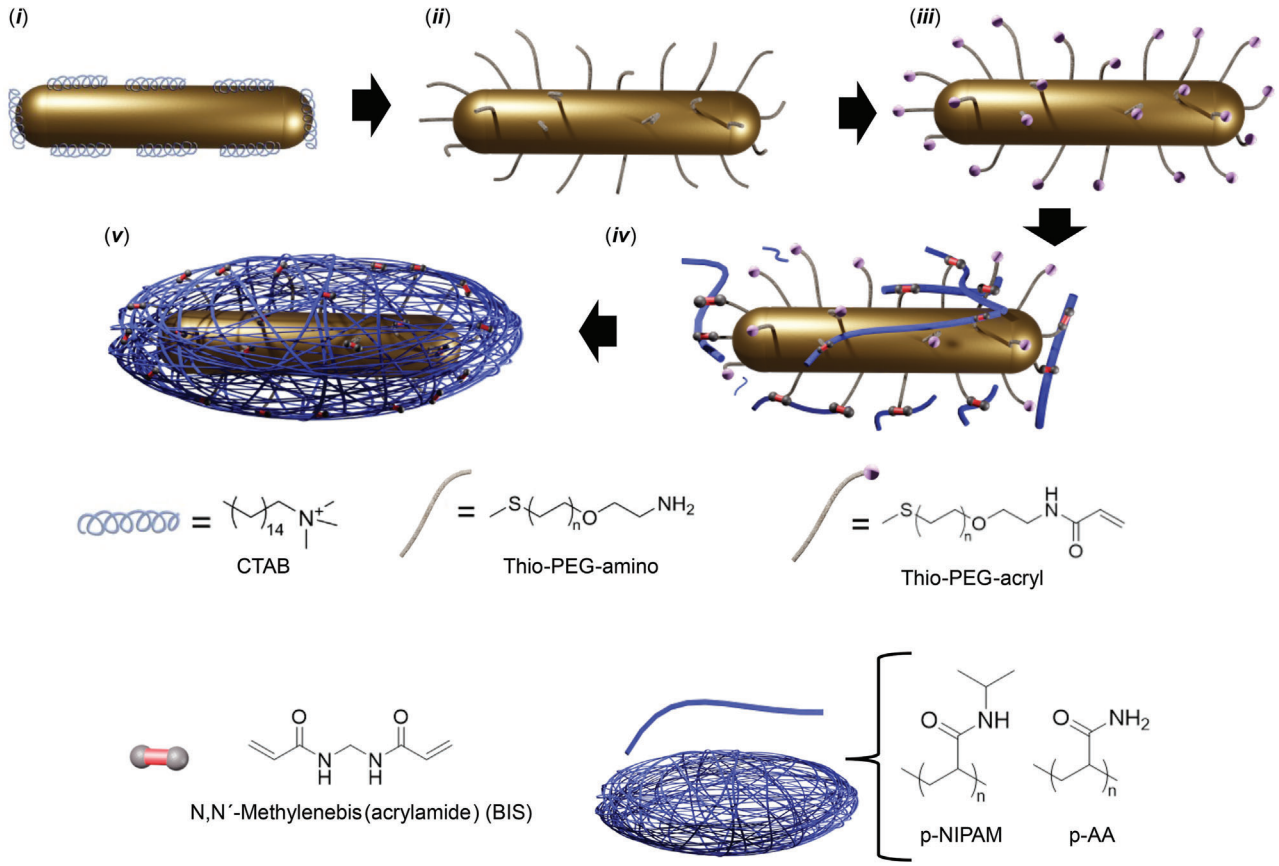

Scheme 1. Synthetic scheme for the one-pot in situ encapsulation of a single AuNP Rod within crosslinked nanogels. The procedure involves i) preparation of Rods with cetyltrimethylammonium bromide (CTAB), ii) full surface grafting with amino-terminated polyethylene glycol (PEG) (MW 5 kDa) chains, and iii) subsequent acryloylation of the external functional groups and the in situ radical polymerization of either acrylamide (AA) or N-Isopropylacrylamide (NIPAM) monomers in the presence of N,N´-methylenebis(acrylamide) (BIS) as a crosslinker. iv) Polymeric (pAA or pNIPAM) growth on the surface of the nanoparticle gives rise to v) complete encapsulation of the Rod within corresponding nanogels.

therapies. Unprotected AuNPs suffer from evaporation and the subsequent condensation of gold atoms, leading to small satellite clusters emerging around the inorganic core upon laser irradiation.[10] As a result, anisotropic AuNPs experience a loss of dimensional attributes, manifesting as a loss in photothermal conversion capacity;[11] therefore, strategies that protect and stabilize anisotropic AuNPs may widen their application as photothermal agents.

Organic polymeric matrices shield and stabilize AuNPs; for example, drug delivery strategies have employed multiple AuNPs embedded in preformed thermoresponsive nanogels based on poly-N-isopropylacrylamide (pNIPAM)-grafted thiolated chitosan.[12] Laser exposure for 10 min decreased the photothermal conversion efficiency from a temperature change of 9 to 5 °C (representing a 1.8-fold reduction), likely due to the high density of the protective nanogel, underscoring the need to fabricate thin-shell protective layers. In a related study, Contreras-Cáceres et al. encapsulated individual AuNPs within thermoresponsive microgels based on the in situ growth of crosslinked pNIPAM,[13] which required the prior encapsulation of AuNPs within polystyrene particles to ensure sufficient stability and prevent aggregation during microgel polymerization; however, the resultant material exhibited an egg-like shape, significantly overpassing the AuNP's initial dimensions. Thus, reported methodologies remain limited regarding the controlled deposition of polymeric networks over the surface of inorganic particles; as a result, the final optical properties of the material cannot be anticipated.[14] Developing methodologies that preserve the morphology remains particularly interesting for anisotropic AuNPs to safeguard their robust plasmonic features.[15]

In this study, we devised a protocol that stabilizes anisotropic AuNPs while preserving their dimensions and, thus, their optical features. Our strategy envisaged one-pot in situ polymeric growth that provides for AuNP encapsulation within the resultant nanogel. The in-depth characterization of our hybrid nanomaterials revealed the encapsulation of single anisotropic AuNPs within nanogels with a 2–8 nm thickness, which preserves their original size and shape. Notably, the optical properties of rod- and star-shaped anisotropic AuNPs remained intact, while showing excellent stability against prolonged near-infrared-light irradiation. We believe that the creation of AuNP-nanogel hybrid nanomaterials can improve the prospects of AuNPs as photothermal agents in the clinic and offer a new avenue for exploring novel functionalization strategies for inorganic nanoparticles.

Table 1. Optimized conditions of ligand exchange, acryloylation, and nanogel formation for the synthesis of spherical isotropic AuNPs as well as rod- and star-shaped anisotropic AuNPs.

Sample material	Ligand Exchange: PEGylation			Acryloylation			Nanogel preparation			
	Molar Ratio (AuNP: HS-PEG5k-NH_2)	Time	Conditions	Molar Ratio (AuNP:NAS)	Time	Conditions	Molar Ratio (AuNP: pAA nanogel)	Molar Ratio (AuNP: pNIPAM nanogel)	Time	Conditions
Spheres 14 nm	1:50000	24 h	Ultra pure H_2O	1:180000	2 h	HEPES buffer (10 mM; pH = 8.52)	1:30000	1:5000000	4 h	Ultra pure H_2O
Spheres 40 nm		48 h								
Rods										
Stars										

2. Results and Discussion

2.1. Synthetic Methodology to Wrap Gold Nanoparticles

2.1.1. Optimization of the Encapsulation Protocol

We took inspiration from our previously reported methodology that successfully wrap individual enzymes within acrylic monomers upon free radical polymerization for our strategy to decorate individual AuNPs within a thin nanogel layer.[16] We envisaged that the growth of a crosslinked polymeric network from the nanoparticle surface would induce the embedding of the inorganic component within a nanogel shell. We anticipated several challenges, such as interparticle aggregation and the loss of colloidal stability during synthesis; for this reason, we envisioned a procedure involving several synthetic steps (**Scheme 1**; Schemes S1–S3, Supporting Information).

As a proof-of-concept, we extensively explored each step using spherical isotropic AuNPs (SPhs), which are more easily produced at high concentrations than anisotropic AuNPs. We carefully assessed parameters such as bifunctional linker composition and length, reagent concentration, reaction times, temperatures, and solvents to reach the optimal parameters described in **Table 1** (Supporting Information provides additional details). Then, we employed the optimal parameters to encapsulate anisotropic AuNPs and 40 nm SPhs. Briefly, we grafted the surface of AuNPs (Scheme 1i) with bifunctional thiolated-polyethylene glycol-amine (PEG) (Scheme 1ii) to provide nanoparticle stability and enable subsequent steps.[17,18] We determined PEG-amino (MW 5.0 kDa) grafting as the most convenient approach to avoid nanoparticle aggregation and enhance long-term colloidal stability (Table S1, Supporting Information). Next, we reacted grafted amino-functionalized linkers with N-acryloylsuccinimide (NAS) to activate the nanoparticle surface (Scheme 1iii).[19] Acryloyl groups serve as anchoring points to build the polymeric network around the AuNP surface, and we achieved optimal results upon 2 h of incubation at room temperature with 0.02 mM NAS (Table S2, Supporting Information). Finally, we subjected activated AuNPs to in situ radical polymerization (Scheme 1iv,v); we finely tuned the protocol to weave thin crosslinked layers of polyacrylamide (pAA) or pNIPAM nanogels around individual nanoparticles, avoiding the aggregation/encapsulation of multiple nanoparticles within the nanogel (Table S3, Supporting Information). We selected optimized conditions following comprehensive physicochemical characterization, which included transmission electron microscopy (TEM), scanning electronic microscopy (SEM), UV–vis spectroscopy, differential scanning calorimetry (DSC), gel permeation chromatography (GPC), and atomic force microscopy (AFM) (**Figure 1**; Figures S1–S6, Supporting Information).

TEM analysis confirmed the successful encapsulation of SPh within thin films (2–3 nm thickness) of a pAA nanogel at an acrylamide-to-SPh molar ratio of 30000:1 (SPh@pAA; Figure 1A; Figure S1, Supporting Information). While higher ratios led to SPh aggregation, lower acrylamide concentrations gave rise to incomplete SPh encapsulation (Figure S2A,B, Supporting Information). When using pNIPAM nanogels (SPh@pNIPAM), complete SPh encapsulation required an N-isopropylacrylamide-to-SPh ratio of 5000000:1 (Section S3.1.2-c.2, Supporting

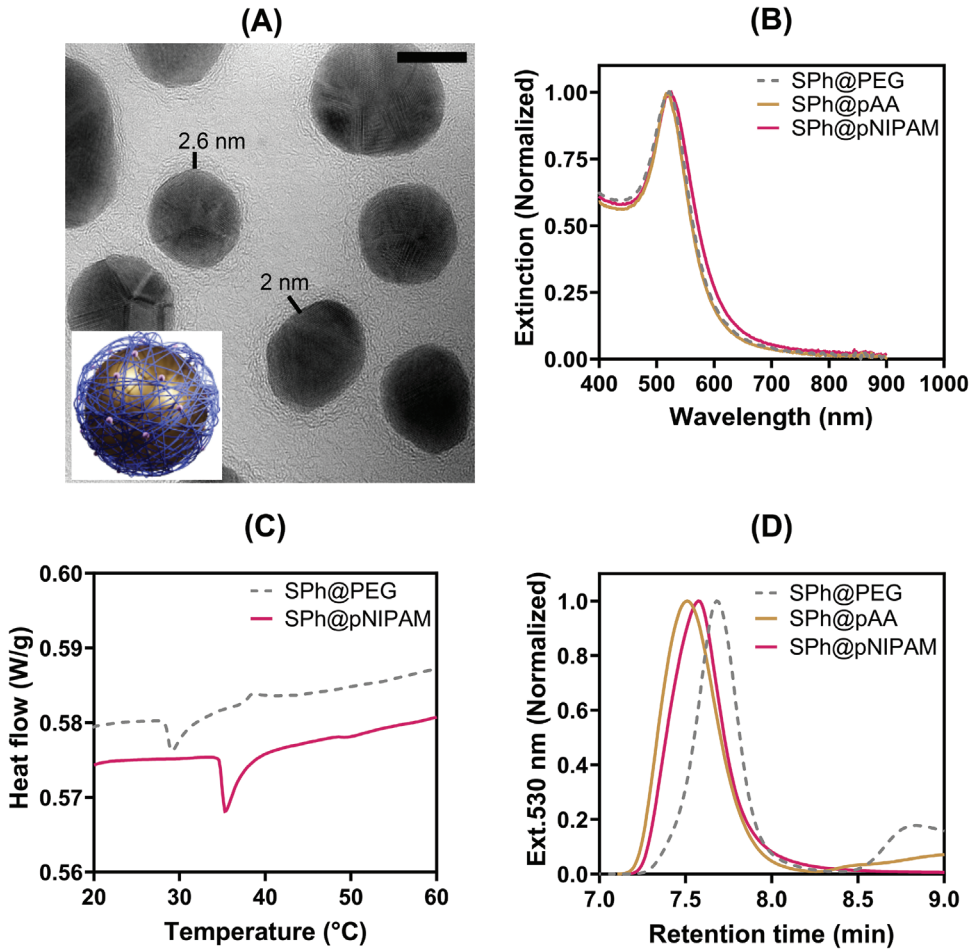

Figure 1. Selected characterization results for PEGylated and nanogel-encapsulated SPh nanoparticles. A) TEM image of SPh@pAA with nanogel thickness highlighted (scale bar 10 nm) (inset showing scheme for SPh). B) Normalized extinction spectra showing localized surface plasmon resonance (LSPR) wavelength for SPh@PEG, SPh@pAA, and SPh@pNIPAM. C) Differential scanning calorimetry thermograms comparing SPh@PEG and SPh@pNIPAM. D) Chromatograms obtained by GPC normalized at 530 nm for SPh@PEG, SPh@pAA, and SPh@pNIPAM.

Information provides detailed information). Our findings revealed that the increased size of SPh nanoparticles did not significantly affect their optical properties, as demonstrated by UV–vis measurements (Figure 1B; Figures S2C–E and S3, Supporting Information). DSC revealed the thermal responsiveness induced by the inclusion of pNIPAM in SPh@pNIPAM; we observed a notable shift from 29 to 35 °C in the DSC peak for non-encapsulated SPh nanoparticles and SPh@pNIPAM, respectively (Figure 1C; Figure S4, Supporting Information). Interestingly, GPC analysis revealed that SPh@pAA and SPh@pNIPAM eluted before PEGylated SPh nanoparticles (SPh@PEG) due to an increase in molecular weight (Figure 1D; Figure S5, Supporting Information). Furthermore, AFM results (Figure S6, Supporting Information) demonstrated a deeper penetration of the tip in terms of height and increased adhesion for encapsulated SPh nanoparticles. This result suggests a greater quantity of polymer present in the case of nanogels. Therefore, the characterization of nanogel-encapsulated SPh nanoparticles confirmed the successful formation of a thin polymer layer around individual nanoparticles under optimized synthesis conditions.

2.1.2. Synthesis and Encapsulation of Rod- and Star-Shaped Anisotropic AuNPs Within Nanogels

After successfully encapsulating individual SPh nanoparticles, we aimed to encapsulate rod-and star-shaped anisotropic AuNPs based on this optimized procedure. The scale employed obliged us to perform several synthesis batches for each desired hybrid nanomaterial to achieve sufficient material for characterization.[17,18] We collected batches with only slight variations in the maximum extinction measured in the visible spectrum. Rod-shaped anisotropic AuNPs displayed maximum absorption peaks at ≈715 nm (within the near-infrared region) and 515 nm, consistent with a predicted axial length of 40 nm and a longitudinal length of ≈10 nm.[17] Star-shaped anisotropic AuNPs displayed broad extinction from the visible to the near-infrared region – 600 to 1000 nm – with maximum absorption at 800 nm corresponding to particles with an average diameter of 40 nm (according to reported information).[18]

We slightly modified the encapsulation protocol to ensure the stability of rod-shaped (Rod@pAA and Rod@pNIPAM) and

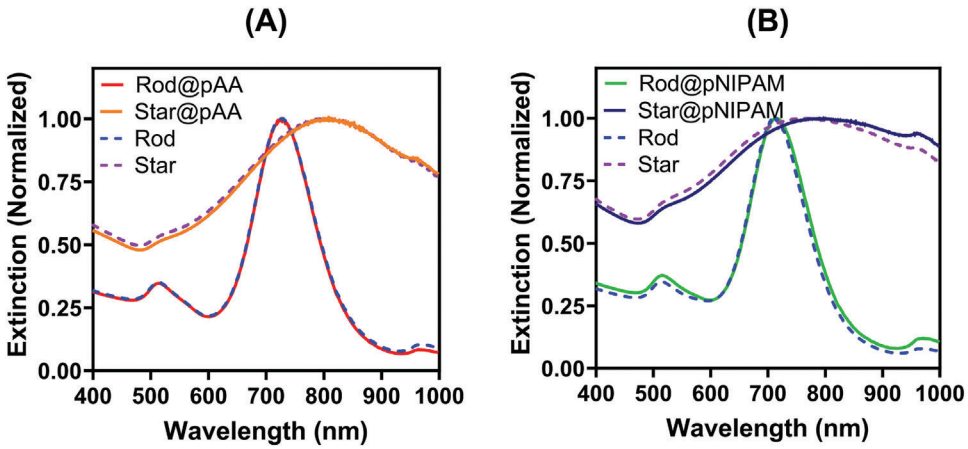

Figure 2. Normalized extinction spectra showing the localized surface plasmon resonance (LSPR) wavelength for rod- and star-shaped anisotropic AuNPs@PEG before (dotted lines) and after encapsulation (continuous lines) within A) pAA and B) pNIPAM nanogels.

star-shaped (Star@pAA and Star@pNIPAM) anisotropic AuNPs; specifically, we employed a prolonged incubation (up to 48 h) with thiolated PEG-amine (with a molar ratio 50000:1 HS-PEG5k-NH_2:AuNPs) for stabilization (compared to the protocol for SPh encapsulation) to achieve complete encapsulation due to the increased surface area and the presence of spikes (Table 1). The remaining synthetic conditions were comparable (with a molar ratio of 180000:1 NAS:AuNPs; 30000:1 AA:AuNPs; and 5000000:1 NIPAM:AuNPs) (Supporting Information provides additional details).

2.1.3. Analysis of the Optical Properties of AuNP-Nanogel Hybrid Nanomaterials

We aimed to stabilize anisotropic AuNPs without affecting their optical properties; typically, the complete encapsulation of AuNPs within a polymer layer results in a noticeable shift in the plasmonic band, manifested by a wavelength variation of several nanometers.[20–23] This shift of the plasmon band maximum suggests an irreversible impact on the optical properties of the nanoparticles. Encouragingly, **Figure 2** reports a lack of significant plasmon shift compared to unencapsulated rod- and star-shaped anisotropic AuNPs, indicating the absence of aggregation and the maintenance of the original optical properties for Rod@pAA and Star@pAA (Figure 2A) or Rod@pNIPAM and Star@pNIPAM (Figure 2B). Thus, we conclude that our approach conserves the optical features of rod- and star-shaped anisotropic AuNPs after nanogel encapsulation.

2.2. Structural Characterization of AuNP-Nanogel Hybrid Nanomaterials

The elucidation of the core-shell configuration of AuNP-nanogel hybrid nanomaterials remains challenging due to the inorganic nature of the nanoparticle and the relative thinness of the organic polymer layer. Here, we thoroughly characterized AuNP-nanogel hybrid nanomaterials to confirm the presence of a thin polymeric layer.

2.2.1. Small-Angle X-ray Scattering Characterization of Nanogel-Encapsulated Anisotropic AuNPs

We employed small-angle X-ray scattering (SAXS) to investigate whether the nanogels retain the shape congruence of the anisotropic inorganic core in solution and, additionally, to verify the existence of the encapsulating organic polymeric layer.

Figure 3A,B depicts SAXS patterns and Normalized Kratky representation curves obtained for Rod@pAA, Rod@pNIPAM, and PEGylated rod-shaped anisotropic AuNPs (Rod@PEG). We employed cylindrical and cylindrical core-shell models to fit the data derived from Rod@PEG and Rod@pAA/Rod@pNIPAM.[24] SAXS patterns obtained for Rod@PEG fit well with the characteristic features typically observed for cylindrical structures, with two subtle inflection points at q ≈0.29 and ≈0.11 nm^{-1}, that corresponded to the transverse and longitudinal axis of the rod, respectively. These data provide an adjusted diameter of 12.2 nm and a length of 40 nm (with a size polydispersity of 10%) for Rod@PEG. From these data, we aimed to determine the shell thickness of the nanogel-encapsulated rod-shaped anisotropic AuNPs. We fixed the electron densities applied for the gold and polymer layer during the fitting to $\rho(Au)/\rho(H_2O)$ ≈10 and $\rho(polymer)/\rho(H_2O)$ ≈1.5, respectively. As shown in Figure 3A, the rod encapsulated by both nanogels presented similar features, albeit with a slight shift toward smaller angles, suggesting a change in the overall hybrid size (≈0.6 nm^{-1} for Rod@pAA and ≈1.4 nm^{-1} for Rod@pNIPAM). As we previously discounted the aggregation of the gold cores (Figure 2), we attributed the observed shift to the polymeric shell formed around rod-shaped anisotropic AuNPs; therefore, the data provide an adjusted shell thickness of 1.5 and 7.0 nm for Rod@pAA and Rod@pNIPAM, respectively. The features observed in the Kratky plots (Figure 3B) align with fitting results. Samples present a main peak located at q ≈0.19 nm^{-1} and a shoulder at q ≈0.8 nm^{-1}. While Rod@pAA exhibits a Kratky plot similar to Rod@PEG, Rod@pNIPAM presents a clear shift of the main features toward lower q-values. This result indicates a thicker pNIPAM shell formed around the rod than pAA, consistent with the fitting results.

Figure 3C,D presents the SAXS curves obtained for Star@pAA/Star@pNIPAM and Star@PEG. The SAXS curves

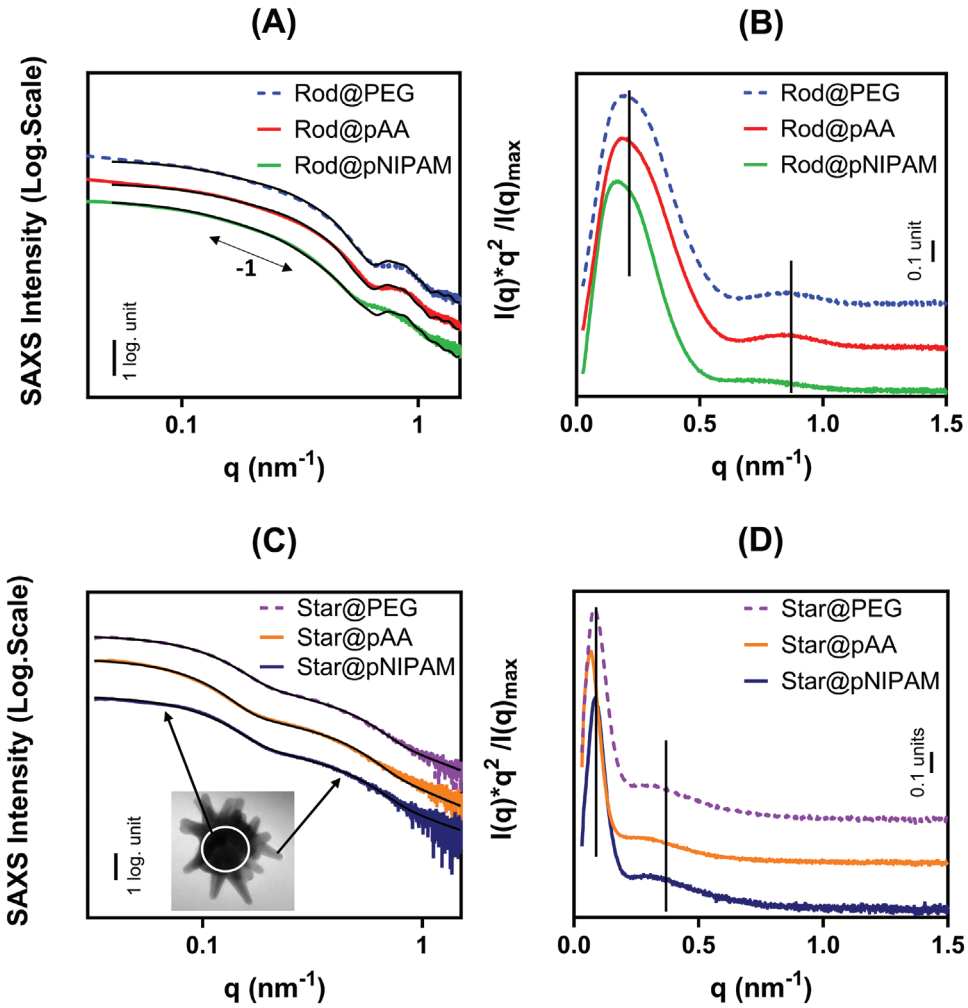

Figure 3. SAXS data for AuNP-nanogel hybrid nanomaterials. A) SAXS patterns (log-log scale) of Rod@PEG, Rod@pAA, and Rod@pNIPAM in stacked representation. Black lines depict adjusted curves using models noted in the main text. The double arrow indicates a slope between the two inflection points of ≈1 due to the 1D geometry of the rod. B) Normalized Kratky representation of SAXS patterns obtained for Rod@PEG, Rod@pAA, and Rod@pNIPAM (stacked curves). C) SAXS patterns (log–log scale) of Star@PEG, Star@pAA, and Star@pNIPAM samples in stacked representation. Black lines correspond to adjusted curves using models mentioned in the main text. D) Normalized Kratky representation of SAXS patterns obtained for Star@PEG, Stars@pAA, and Star@pNIPAM (stacked curves).

possess two distinctive regions compatible with a non-regular star (bumps at lower [from overall size contribution] and higher angles [from the edges of the star]). Representation through a geometrical analytical model remains challenging considering the shape of these nanoparticles; therefore, we used the Beaucage model to fit the obtained data.[25] This model uses levels with contributions stemming from their radius of gyration (Rg) and Porod exponent; therefore, we can fit star-shaped nanoparticles using two levels, a larger one for the overall size of the star and a smaller one for the spikes (as shown by the inset TEM image in Figure 3C). The black lines in Figure 3C represent the best fits obtained for Star@pAA, Star@pNIPAM, and Star@PEG. Thus, Star@PEG can be adjusted by applying an Rg of ≈21.3 and ≈5.0 nm; Star@pAA with a Rg of ≈25.3 and ≈5.6 nm; and Star@pNIPAM with a Rg of ≈22.1 and ≈5.1 nm. Size analysis results provided a diameter of ≈42.6, ≈50.6, and ≈44.2 nm for Star@PEG, Star@pAA, and Star@pNIPAM. Kratky plots of these samples (Figure 3D) also provide valuable information regarding the distribution of the polymeric network over the irregular surface of star-shaped anisotropic AuNPs. If the polymeric network grows homogeneously over the surface, maintaining shape congruence, the peak of Star@PEG at lower q values (i.e., ≈0.09 nm^{-1}) will shift to lower values;[26] meanwhile, if the polymeric network accumulates into the spaces between edges, the shoulder at ≈0.28 nm^{-1} will be affected.[27] This latter case would prompt the loss of the initial shape, potentially leading to the formation of a spherical-like external shell in solution. Unlike the results for Rod@pAA and Rod@pNIPAM, we found significant differences when comparing the Kratky representation of Star@pAA and Star@pNIPAM, most likely due to the thin polymeric layer achieved for Rod@pNIPAM. As for Star@pAA, noticeable shifts toward lower q-values (Δq ≈ 0.02 nm^{-1}) were observed for both the peak and shoulder. These findings indicate comprehensive coverage of the nanoparticle, with a significant accumulation between the spikes, suggesting the presence of a thick layer surrounding the nanoparticle.

In conclusion, SAXS measurements confirmed polymer growth on the surface of rod- and star-shaped anisotropic AuNPs, with the robust fitting of applied models providing evidence for the maintenance of morphology after encapsulation.

2.2.2. Transmission Electron Microscopy Characterization of Nanogel-Encapsulated Anisotropic AuNPs

The accurate observation of AuNP-nanogel hybrid nanomaterials represents a challenging task due to the minuscule thickness of the polymeric layer wrapping the AuNPs, coupled with the anisotropic nature of AuNPs, which could potentially hinder complete encapsulation. Achieving complete coverage would substantially enhance photothermal therapy techniques utilizing anisotropic AuNPs.[28–30] Here, we assessed the presence of a nanogel shell surrounding anisotropic AuNPs (conserving their geometric configuration) by TEM; overall, our approach supported the complete encapsulation of AuNPs (**Figure 4**).

While we could not observe grafted linear PEGs on Rod@PEG (Figure 4A), we did detect a thin organic coating ranging from 0.6 to 2 nm in thickness for Star@PEG (Figure 4B), likely due to the formation of a more dense polymer layer. This observation agrees with a previous study describing how AuNPs coated with 5 kDa PEG ligands displayed an increase in organic layer thickness of ≈2 nm.[31] Upon polymerization and subsequent in situ encapsulation, Rod@pAA possessed a uniform organic layer of ≈3 nm (Figure 4C) across the nanoparticle surface, providing a fully encapsulating nanogel shell; meanwhile, Star@pAA possessed a more compact polymeric layer with a thickness of ≈2 nm on spikes and 4–6 nm on spike junctions, which confirms the complete encapsulation of AuNPs by pAA (Figure 4D). TEM images corresponding to Rod@pNIPAM and Star@pNIPAM displayed comparable features, although slightly thicker (Figure 4E,F); therefore, the TEM study confirmed the formation of densely packed organic shells due to nanogel crosslinking.

We consistently found similar outcomes for SAXS and TEM, which provided comparable diameters for the AuNP-nanogel hybrid nanomaterials. These results indicate that nanogel swelling remains limited, likely due to a high density of crosslinkers; however, despite the variations observed among the techniques, all results converge toward a consistent trend. Any discrepancies may stem from the underlying physical principles inherent to each measurement, and the interpretation of each outcome may be challenging, given the intricate topology of the nanoparticle.

2.2.3. Thermoresponsive Characterization of Anisotropic AuNPs Encapsulated by pNIPAM Nanogels

The in situ formation of a pNIPAM shell surrounding anisotropic AuNPs can be determined by corresponding DSC thermograms, as according to the reported literature, pNIPAM and HS-PEG5k display a peak at 33–34 °C.[32,33] These values derive from the intrinsic transition temperature for pNIPAM, but as a consequence of a conformational change of their chains (from coiled to globular) for PEG; however, the presence of AuNPs can alter this peak (depending on shape and concentration).[34] The encapsulation of rod-shaped anisotropic AuNPs within a pNIPAM nanogel induced a shift of an exothermic peak from 33.49 °C (Rods@PEG) to 34.64 °C (Rods@pNIPAM), with an associated drop in the crystallization enthalpy from −57.71 to −50.04 mJ g^{-1}, respectively (**Figure 5**A). These values indicate a significant change in the transition phase of nanoparticle-grafted polymers, most likely due to the presence of thermoresponsive pNIPAM in this hybrid nanomaterial. This thermoresponsive polymer employs a portion of the energy required to generate the DSC peak to change its conformation, leading to a more positive crystallization enthalpy; consequently, the transition of the material toward a more organized state requires a significant amount of energy. Similarly, analysis of star-shaped anisotropic AuNPs within a pNIPAM nanogel revealed enthalpy values of −77.11 mJ g^{-1} for Star@PEG and −58.80 mJ g^{-1} for Star@pNIPAM (Figure 5B), suggesting a less exothermic process in the presence of the pNIPAM shell, likely due to the thermoresponsive nature of the polymer. The findings agree with existing literature, which consistently describes negative heat flow values for PEGylated AuNPs and positive values for pNIPAM-coated AuNPs;[34,35] furthermore, previous DSC studies have indicated that PEG reduces the enthalpy of pNIPAM.[36] These findings confirm the successful synthesis of thermoresponsive AuNP-nanogel hybrid nanomaterials with tailored properties, which could have diverse applications in various fields.

2.3. AuNP-Nanogel Hybrid Nanomaterial Stability During Laser-Into-Heat Conversion Upon Laser Irradiation

The stabilization techniques typically employed for AuNPs during laser irradiation often encounter a bottleneck (as described above), adversely affecting their inherent optical properties; in this context, we introduced our hybrid nanomaterial approach as a promising enhancement. We thoroughly evaluated the ability of our AuNP-nanogel hybrid nanomaterials to function as efficient light-to-heat converters, a critical characteristic for their potential application in photothermal therapy. AuNP-nanogel hybrid nanomaterials must consistently maintain their plasmon band within the near-infrared wavelength after irradiation to ensure their therapeutic effectiveness. Incorporating anisotropic AuNPs into nanogels may hinder AuNP aggregation and modification of morphological traits (e.g., a shift toward a spherical shape); overall, these common phenomena have been extensively documented and compromise optical properties.[37,38]

We irradiated nanogel-encapsulated rod- and star-shaped anisotropic AuNPs with a 785 nm laser at an 1980 mW cm^{-2} intensity. We monitored the solution temperature using a thermal camera; each experiment consisted of a 30-min laser exposure followed by a 30-min gap repeated three times (a 3-h experiment). We subjected our AuNP-nanogel hybrid nanomaterials to prolonged laser irradiation to demonstrate their ability to maintain high-temperature conversion over extended periods, pushing the characterization and stability tests to the limit; this characteristic could ensure the effective ablation of tumors in a hypothetical photothermal therapy scenario.

Upon exposure of our AuNP-nanogel hybrid nanomaterials to laser irradiation (**Figure 6**A–C shows a representative example), we recorded heating curves (Figure 6D,E) and UV–vis spectra (Figure 6F,G) before and after irradiation (**Table 2** provides a summary of the data). We employed SPh@PEG with diameters of 14

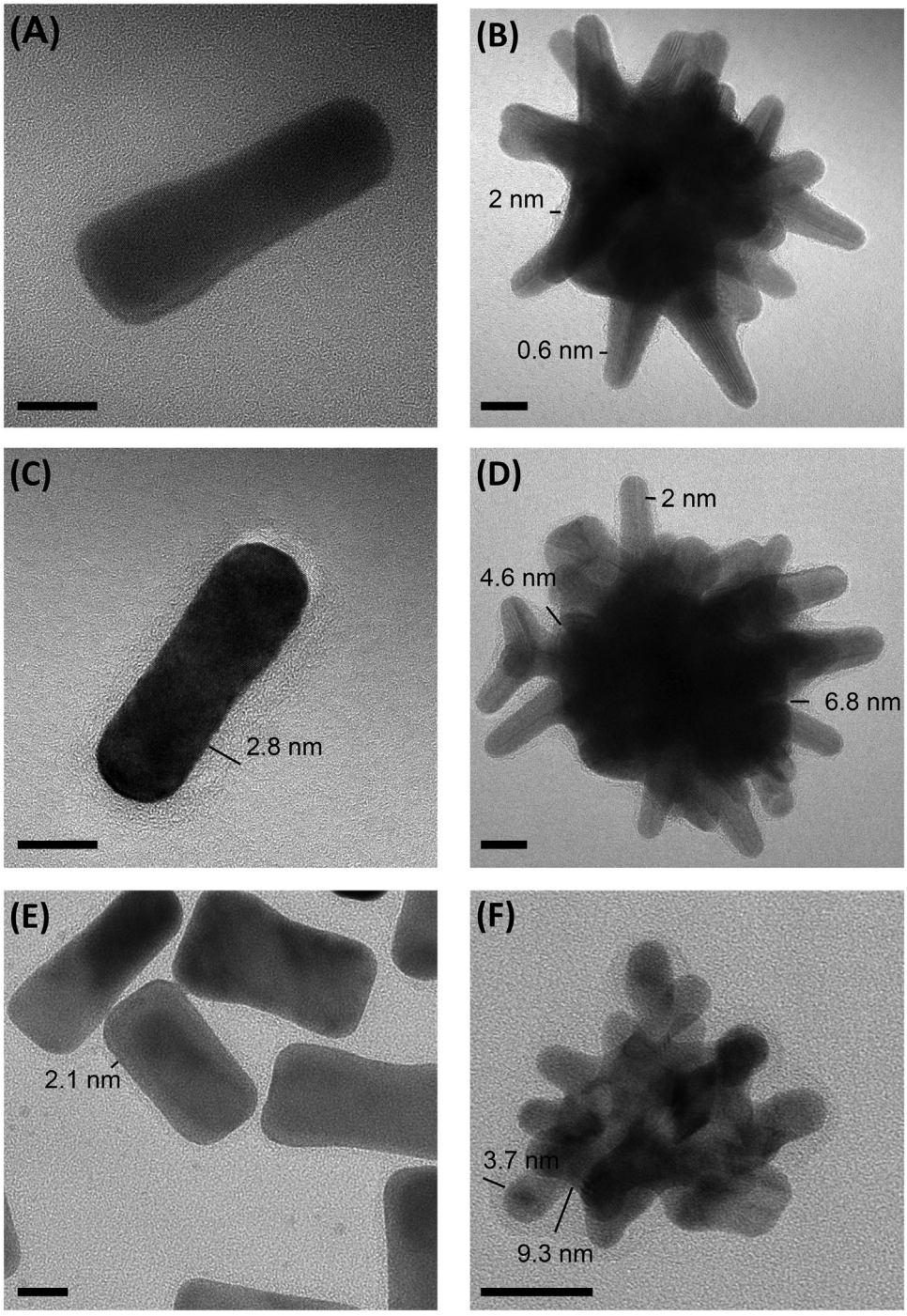

Figure 4. Transmission electron microscopy images of A) Rod@PEG, B) Star@PEG, C) Rod@pAA, D) Star@pAA, E) Rod@pNIPAM, and F) Star@pNIPAM. Polymeric thicknesses highlighted in nm. Scale bars = 10 nm.

and 40 nm as a negative control; SPh@PEG maintained their structural integrity according to the UV–vis measurements, as irradiation did not alter the plasmonic band, although (as expected) we did not measure any significant photothermal conversion capacity at 530 nm (Figure S8, Supporting Information).

We revealed significant disparities when plotting the heating curves for nanogel-encapsulated rod- and star-shaped anisotropic AuNPs. We first observed that non-encapsulated anisotropic AuNPs underwent a noticeable decrease in the efficiency of laser-to-heat conversion. In the first cycle of irradiation (Figure 6D, blue discontinuous line), non-encapsulated rods achieved a remarkable temperature peak of 63 °C; however, this efficiency decreased in subsequent cycles (particularly by the third cycle), resulting in a maximum temperature of 47 °C. In the case of

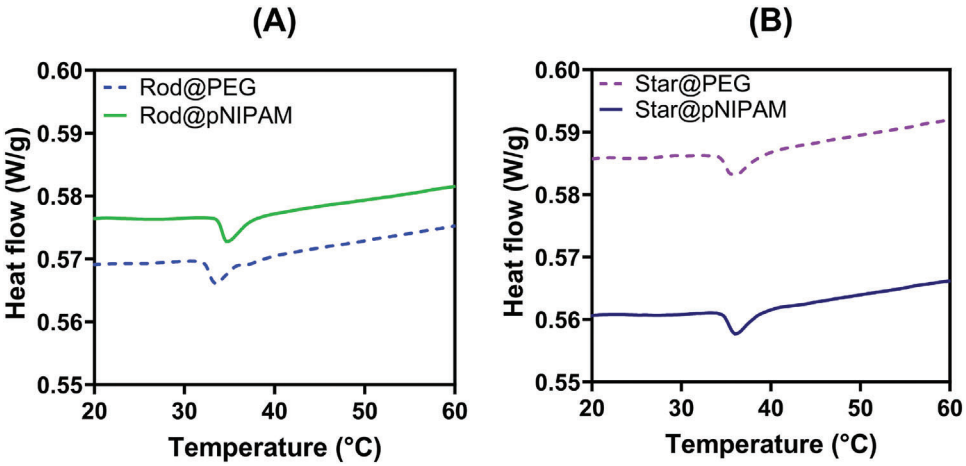

Figure 5. Differential scanning calorimetry thermograms for A) Rod-shaped and B) Star-shaped AuNPs grafted with PEG or encapsulated by pNIPAM. Isotherms were performed at a heating rate of 10 °C min^{-1} under N_2 flow at 50 mL min^{-1}.

non-encapsulated stars, we observed a reduction of 5 °C between the first and the third cycles (Figure 6E, pink discontinuous line). We observed maximum achieved temperatures that agreed with the reported literature.[39] Encapsulating AuNPs within nanogels to form hybrid nanomaterials could significantly enhance stability when subjected to laser irradiation, which relies on the characteristics of the polymers employed. Rod@pAA (Figure 6D, red line) and Star@pAA (Figure 6E, orange line) exhibited high photothermal conversion efficacy across all three irradiation cycles. Throughout these cycles, we observed a minor variation of 1 °C from the maximum, which indicates a consistent and stable response to the laser irradiation and makes the pAA nanogel an excellent choice for this application. Conversely, the heating curves yielded unexpected results when we used a pNIPAM nanogel for encapsulation. The temperature fluctuated during the three irradiation cycles for Rod@pNIPAM (Figure 6D, green line) and Star@pNIPAM (Figure 6D, purple line) – Rod@pNIPAM experienced a significant drop of 24 °C (from 58 to 34 °C) during the second irradiation cycle while Star@pNIPAM experienced an even more substantial drop of 37 °C (from 65 to 28 °C) during the first heating cycle. Star@pNIPAM recovered the temperature drop to 51 °C during the second heating cycle, and we observed a rapid increase of 17 °C (from 53 to 70 °C) during the third heating cycle. To further validate these fluctuations, we prepared a fresh batch of hybrids and replicated the experiment. The corroborating results (Figure S8, Supporting Information), affirm our initial observations. These results may be attributed to the thermoresponsive behavior of pNIPAM – the hydrophobic nature of pNIPAM may decrease the aqueous dispersability of the hybrid nanomaterial as the temperature increases above the transition temperature, which in turn decreases photothermal conversion efficacy. These fluctuations suggest that a pNIPAM nanogel may not maintain consistent photothermal conversion under laser irradiation to the same degree as pAA nanogels.

We also evaluated the plasmon band of nanogel-encapsulated rod- and star-shaped anisotropic AuNPs to assess the impact of irradiation on the morphology of these hybrid nanomaterials. The plasmon bands of unencapsulated rods and stars experienced hypsochromic shifts of 50 nm (Figure 6F, blue lines) and 99 nm (Figure 6G, pink lines) after irradiation, which agrees with earlier reports of the deterioration of anisotropic PEGylated AuNPs into spherical aggregates after prolonged exposure to laser radiation.[40]

Significant efforts have recently aimed to safeguard anisotropic AuNPs during laser exposure; for instance, a protective polypyrrole shell enhanced the stability and laser-to-heat conversion efficiency of AuNPs by 20%.[41] Unfortunately, this shell caused a hypsochromic shift in the plasmonic band, affecting the optical properties and indicating limited control over synthesis. Coating AuNPs with a silica shell represents a common method to improve stability under laser irradiation;[40] however, the plasmonic band shifts slightly after 3 min of exposure to a 1064 nm laser, suggesting the unsuitability of this method for long-term experiments due to reduced photothermal efficiency. These findings underscore the limitations of traditional stabilization methods that use linear polymers to maintain the shape of AuNPs during irradiation. In our study, the encapsulation of anisotropic AuNPs within nanogels prompted a significant improvement in the preservation of nanoparticle shape. Plasmon bands (denoted with "_B" to indicate before irradiation a "_A" for after irradiation) shifted only 7 nm for Rod@pAA (Figure 6F, red lines) and 71 nm for Star@pAA (Figure 6G, orange lines) compared to unencapsulated rod and star analogs. Surprisingly, we observed no plasmon band shift for Rod@pNIPAM (Figure 6F, green lines) and only a 21 nm shift for Star@pNIPAM (Figure 6G, purple lines), indicating that pNIPAM holds great promise in protecting nanoparticle morphology. Overall, the UV–vis spectra after irradiation highlighted how nanogel encapsulation of anisotropic AuNPs to form hybrid nanomaterials prompted a significant improvement in morphological preservation.

3. Conclusion

We fine-tuned the synthetic procedure to encapsulate individual gold nanoparticles based on the on-surface radical polymerization and growth of thin pAA and pNIPAM nanogels. Optimized conditions could be applied to successfully synthesize ultra-thin

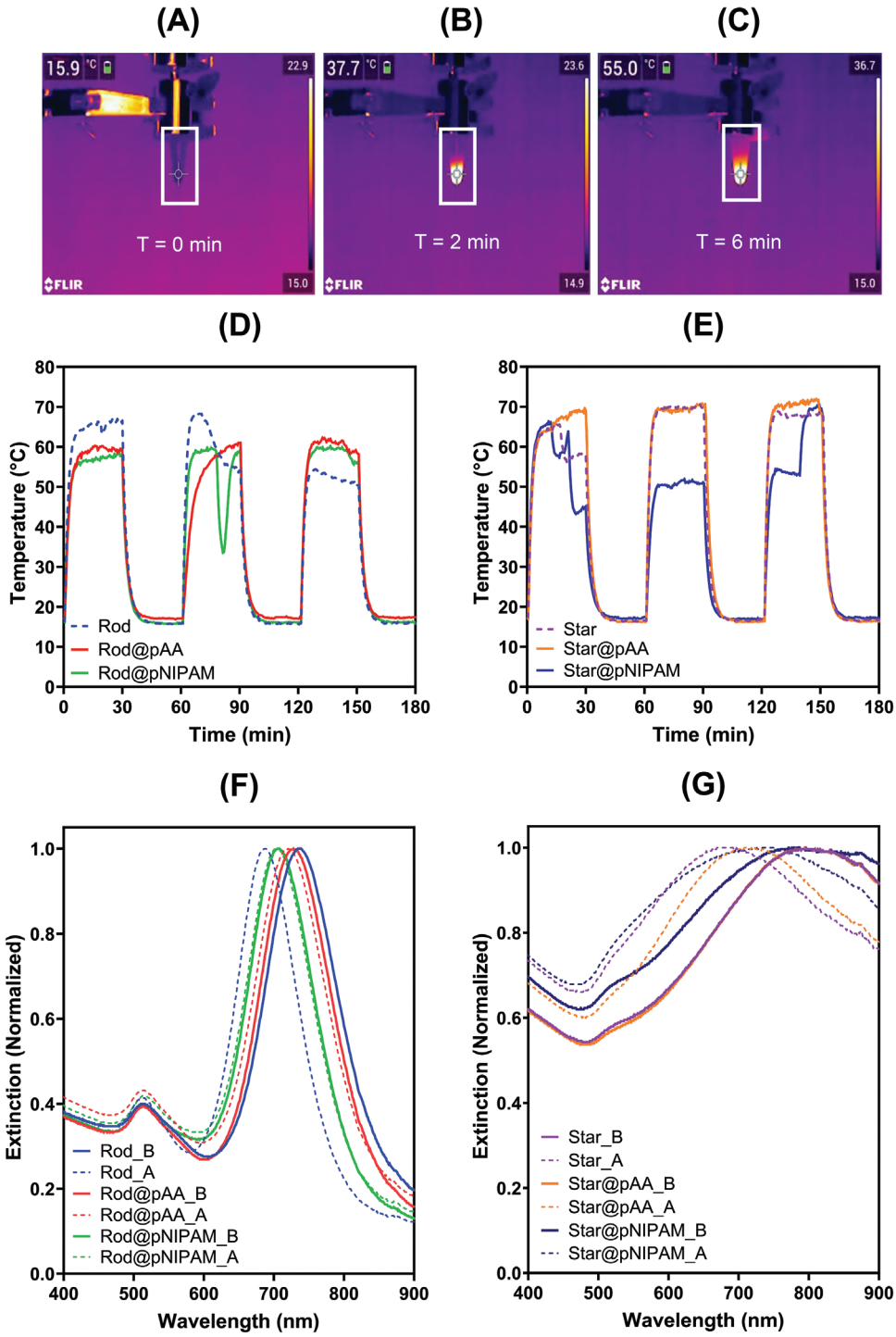

Figure 6. Photothermal conversion capacity of AuNP-nanogel hybrid nanomaterials. A–C) Thermal camera images at selected times of Rod@pAA during laser irradiation as a representative example. D) Heating curves for Rods during laser irradiation. E) Heating curves for Stars during laser irradiation. F) Normalized extinction spectra showing the localized surface plasmon resonance (LSRP) wavelength for Rods, indicating "_B" for spectra before irradiation and "_A" for spectra after irradiation. G) Normalized extinction spectra showing the localized surface plasmon resonance (LSRP) wavelength for Stars, indicating "_B" for spectra before irradiation and "_A" for spectra after irradiation.

Table 2. Summary of relevant data from laser irradiation analysis of materials.

Material	ΔT [°C][a]	Hypsochromic shift [$\Delta\lambda$ = nm][b]
Rod	16	50
Rod@pAA	1	7
Rod@pNIPAM	2	0
Star	5	99
Star@pAA	1	71
Stars@pNIPAM	4	21

[a] Difference between the maximum temperature achieved from the first to the third irradiation curves; [b] Determined by UV–vis spectroscopy.

nanogels that encapsulated a single anisotropic AuNP, increasing the total thickness to 2–8 nm. Complete characterization of hybrids confirmed the presence of a polymer nanogel on the particle surface. High-resolution TEM revealed an anisotropic nanogel thickness shell ranging from ≈2 to 8 nm for star-shaped nanoparticles, characterized by enhanced polymer accumulation between spikes. Conversely, rod-shaped nanoparticles exhibited a uniform yet anisotropic shell thickness spanning ≈2–3 nm. The absence of a non-plasmonic shift in the optical properties indicated the presence of a sufficiently thin polymeric shell to exert negligible optical influence. Furthermore, employing sophisticated SAXS models, we confirmed the presence of the thin polymeric shell and the maintenance of shape congruence in solution.

Upon near-infrared laser irradiation, AuNP-nanogel hybrid nanomaterials exhibited enhanced AuNP stability and efficient light-to-heat conversion, even over extended irradiation periods. Notably, pAA nanogels displayed optimal photothermal conversion efficiency, while pNIPAM nanogels provided superior AuNP protection, as observed by their plasmonic shift after laser irradiation. Overall, our findings suggest that our ultra-thin pAA and pNIPAM nanogels represent promising candidates for the protection of anisotropic AuNPs during laser irradiation; all tested materials reduced the plasmon band shift while maintaining the photothermal capacity of the inorganic core. Indeed, our study demonstrates the superior efficacy of thin nanogels over commonly employed PEG-ligand protection for AuNPs. Specifically, our investigation revealed that the rod-shaped hybrid exhibited the most favorable characteristics for photothermal therapy. Notably, we observed no shift in the plasmonic band when utilizing pNIPAM-based nanogels and only a minimal 7 nm shift with pAA-based nanogels compared to a significant 50 nm shift observed with PEG as the protective ligand. These findings describe remarkably enhanced stabilization values of 50-fold and 7-fold, respectively.

In summary, our synthetic methodology offers a promising approach to stabilize AuNPs for biomedical applications. By grafting the surface of nanogels with various monomers, we anticipate that our materials will withstand complex biological media, thereby enhancing AuNP stability under hazardous biological conditions such as those involving protein interactions or the mucus layer. The influence of morphology on AuNP fate remains largely unexplored as most reported systems report a spherical morphology; hence, our synthetic methodology could enable the systematic analysis of how AuNP geometry impacts the interactions between AuNP-nanogel hybrid nanomaterials and biological barriers.

Supporting Information

Supporting Information is available from the Wiley Online Library or from the author.

Acknowledgements

This research was funded by the Basque Health Department (projects 2023333010 and 2023333023), the University of the Basque Country (projects COLLAB22/05 and GIU21/033), the Spanish Research Agency (PID2022-142128NB-I00 funded by MCIN/ AEI/10.13039/501100011033/ and by the "European Union NextGenerationEU/PRTR"; RYC2018-025923-I from RyC program – MCIN/ AEI /10.13039/501100011033 and FSE "invierte en tu futuro"; "María de Maeztu" Programme for Center of Excellence in R&D, grant CEX2023-001303-M funded by MICIU/AEI/ 10.13039/501100011033), IKERBASQUE-Basque Foundation for Science, and ALBA Synchrotron Light source, Barcelona, Spain (project ID 2023027439). The authors thank S. GIker (UPV/EHU) for the technical and human support. A.S.P. thanks UNLP and CONICET for their support. A.S.P. is a staff member of CONICET. The authors would like to thank Dr. Stuart P. Atkinson and Dr. Andoni Rodríguez-Abetxuko for their collaboration in the revision of the manuscript. They also gratefully thank Aitor Ontoria and Jackeline Soto Cruz for bringing and caring for the samples at the ALBA synchrotron.

Conflict of Interest

The authors declare no conflict of interest.

Author Contributions

D.E.U., A.B., and M.C. conceived the idea and project. D.E.U. synthesized, optimized, and characterized (by UV–vis, Fluorescence, GPC, SEM, AFM, and laser irradiation) all materials. C.H.I. and A.S.P. performed the SAXS measurements, posterior analysis, and data discussion. TEM and DSC were performed by an external service. D.E.U. wrote the first draft of the manuscript. A.B. and M.C. revised and improved the manuscript. A.B. and M.C. supervised and managed the project. All authors approved the final version of the manuscript. The authors declare no competing interests.

Data Availability Statement

The data that support the findings of this study are available from the corresponding author upon reasonable request.

Keywords

gold nanoparticles, nanogels, near-infrared light, photothermal conversion, polymers

Received: May 21, 2024
Revised: July 30, 2024
Published online: September 2, 2024

[1] M. Falahati, F. Attar, M. Sharifi, A. A. Saboury, A. Salihi, F. M. Aziz, I. Kostova, C. Burda, P. Priecel, J. A. Lopez-Sanchez, S. Laurent, N. Hooshmand, M. A. El-Sayed, *Biochim. Biophys. Acta – Gen. Subj.* **2020**, *1864*, 129435.

[2] E. C. Dreaden, A. M. Alkilany, X. Huang, C. J. Murphy, M. A. El-Sayed, *Chem. Soc. Rev.* **2012**, *41*, 2740.
[3] J. Kimling, M. Maier, B. Okenve, V. Kotaidis, H. Ballot, A. Plech, *J. Phys. Chem. B* **2006**, *110*, 15700.
[4] A. Sánchez-Iglesias, J. Barroso, D. M. Solís, J. M. Taboada, F. Obelleiro, V. Pavlov, A. Chuvilin, M. Grzelczak, *J. Mater. Chem. A* **2016**, *4*, 7045.
[5] M. D'Acunto, *Materials* **2018**, *11*, 882.
[6] H.-G. Jin, W. Zhong, S. Yin, X. Zhang, Y.-H. Zhao, Y. Wang, L. Yuan, X.-B. Zhang, *ACS Appl. Mater. Interfaces* **2019**, *11*, 3800.
[7] S. Shen, H. Tang, X. Zhang, J. Ren, Z. Pang, D. Wang, H. Gao, Y. Qian, X. Jiang, W. Yang, *Biomaterials* **2013**, *34*, 3150.
[8] Y. Liu, E. Chorniak, R. Odion, W. Etienne, S. K. Nair, P. Maccarini, G. M. Palmer, B. A. Inman, T. Vo-Dinh, *Nanophotonics* **2021**, *10*, 3295.
[9] A. R. Rastinehad, H. Anastos, E. Wajswol, J. S. Winoker, J. P. Sfakianos, S. K. Doppalapudi, M. R. Carrick, C. J. Knauer, B. Taouli, S. C. Lewis, A. K. Tewari, J. A. Schwartz, S. E. Canfield, A. K. George, J. L. West, N. J. Halas, *Proc. Natl. Acad. Sci.* **2019**, *116*, 18590.
[10] S. Hashimoto, T. Katayama, K. Setoura, M. Strasser, T. Uwada, H. Miyasaka, *Phys. Chem. Chem. Phys.* **2016**, *18*, 4994.
[11] F. Mafuné, J. Kohno, Y. Takeda, T. Kondow, *J. Phys. Chem. B* **2001**, *105*, 9050.
[12] F. Howaili, E. Özliseli, B. Küçüktürkmen, S. M. Razavi, M. Sadeghizadeh, J. M. Rosenholm, *Front. Chem.* **2021**, *8*, 602941.
[13] R. Contreras-Cáceres, A. Sánchez-Iglesias, M. Karg, I. Pastoriza-Santos, J. Pérez-Juste, J. Pacifico, T. Hellweg, A. Fernández-Barbero, L. M. Liz-Marzán, *Adv. Mater.* **2008**, *20*, 1666.
[14] W. Sun, J. Zhang, C. Zhang, Y. Zhou, J. Zhu, C. Peng, M. Shen, X. Shi, *J. Mater. Chem. B* **2018**, *6*, 4835.
[15] Q. Li, X. Qiao, F. Wang, X. Li, J. Yang, Y. Liu, L. Shi, D. Liu, *Anal. Chem.* **2019**, *91*, 13633.
[16] A. Rodriguez-Abetxuko, A. Reifs, D. Sánchez-deAlcázar, A. Beloqui, *Angew. Chem., Int. Ed.* **2022**, *61*, 202206926.
[17] L. Scarabelli, A. Sánchez-Iglesias, J. Pérez-Juste, L. M. Liz-Marzán, *J. Phys. Chem. Lett.* **2015**, *6*, 4270.
[18] D. Jimenez de Aberasturi, A. B. Serrano-Montes, J. Langer, M. Henriksen-Lacey, W. J. Parak, L. M. Liz-Marzán, *Chem. Mater.* **2016**, *28*, 6779.
[19] A. Beloqui, S. Baur, V. Trouillet, A. Welle, J. Madsen, M. Bastmeyer, G. Delaittre, *Small* **2016**, *12*, 1716.
[20] N. A. Harun, M. J. Benning, B. R. Horrocks, D. A. Fulton, *Nanoscale* **2013**, *5*, 3817.
[21] A. J. Vreugdenhil, K. K. Pilatzke, J. M. Parnis, *J. Non.-Cryst. Solids* **2006**, *352*, 3879.
[22] Z. Wei, C.-H. Liu, H. Duan, Q. Luo, M. Huang, S. Thanneeru, M.-P. Nieh, J. He, *Giant* **2022**, *10*, 100102.
[23] J. Song, P. Huang, X. Chen, *Nat. Protoc.* **2016**, *11*, 2287.
[24] J. S. Pedersen, *Adv. Colloid Interface Sci.* **1997**, *70*, 171.
[25] G. Beaucage, *J. Appl. Crystallogr.* **1996**, *29*, 134.
[26] F. E. Galdino, A. S. Picco, L. B. Capeletti, J. Bettini, M. B. Cardoso, *Nano Lett.* **2021**, *21*, 8250.
[27] P. Batat, Ç. Bilir, T. Erdogan, A. Levent Demirel, *Eur. Polym. J.* **2014**, *54*, 79.
[28] B. Li, Q. Xu, X. Li, P. Zhang, X. Zhao, Y. Wang, *Carbohydr. Polym.* **2019**, *203*, 378.
[29] E. Cazares-Cortes, C. Wilhelm, J. E. Perez, A. Espinosa, S. Casale, A. Michel, A. Abou-Hassan, C. Ménager, *Chem. Commun.* **2021**, *57*, 5945.
[30] A. L. Porta, A. Sánchez-Iglesias, T. Altantzis, S. Bals, M. Grzelczak, L. M. Liz-Marzán, *Nanoscale* **2015**, *7*, 10377.
[31] D. B. Chithrani, *J. Nanomed. Res.* **2014**, *1*, 27.
[32] Y. Gao, J. Yang, Y. Ding, X. Ye, *J. Phys. Chem. B* **2014**, *118*, 9460.
[33] K. Pielichowski, K. Flejtuch, *Polym. Adv. Technol.* **2002**, *13*, 690.
[34] R. Yadav, S. Kumar, P. Narang, P. Venkatesu, *J. Colloid Interface Sci.* **2021**, *582*, 478.
[35] M. A. Aboudzadeh, J. Kruse, M. Sanromán Iglesias, D. Cangialosi, A. Alegria, M. Grzelczak, F. Barroso-Bujans, *Soft Matter* **2021**, *17*, 7792.
[36] J. E. Sayed, C. Lorthioir, P. Perrin, N. Sanson, *Soft Matter* **2019**, *15*, 963.
[37] K. K. Kim, H. J. Kwon, S. K. Shin, J. K. Song, S. M. Park, *Chem. Phys. Lett.* **2013**, *588*, 167.
[38] M. Klekotko, J. Olesiak-Banska, K. Matczyszyn, *J. Nanopart. Res.* **2017**, *19*, 327.
[39] B. Gong, Y. Shen, H. Li, X. Li, X. Huan, J. Zhou, Y. Chen, J. Wu, W. Li, *J. Nanobiotechnol.* **2021**, *19*, 41.
[40] G. P. Luke, A. Bashyam, K. A. Homan, S. Makhija, Y.-S. Chen, S. Y. Emelianov, *Nanotechnology* **2013**, *24*, 455101.
[41] J. Li, J. Han, T. Xu, C. Guo, X. Bu, H. Zhang, L. Wang, H. Sun, B. Yang, *Langmuir* **2013**, *29*, 7102.